


# Insights into the self-assembly steps of cyanuric acid toward rosette motifs: a DFT study

Andre N. Petelski<sup>1,2</sup> · Nélica M. Peruchena<sup>2,3</sup> · Silvana C. Pamies<sup>1</sup> · Gladis L. Sosa<sup>1,2</sup> 

Received: 10 February 2017 / Accepted: 19 July 2017  
© Springer-Verlag GmbH Germany 2017

**Abstract** The nature of non-covalent interactions in self-assembling systems is a topic that has aroused great attention in literature. In this field, the 1,3,5-triazinane-2,4,6-trione or cyanuric acid (CA) is one of the most widely used molecules to formulate self-assembled materials or monolayers. In the present work, a variety of molecular aggregates of CA are examined using three different DFT functionals (B3LYP, B3LYP-D3, and  $\omega$ -B97XD) in the framework of the quantum theory of atoms in molecules (QTAIM) and natural bond orbital (NBO) analysis. Herein, a step by step aggregation path is proposed and the origin of cooperative effects is also examined. It is shown that a greater cooperativity is not always associated with a greater binding energy, and the greatest cooperative effect occurs with highly directional hydrogen

bonds. The intramolecular charge transfers play a key role in this effect.

**Keywords** Non-covalent · Self-assembly · Cooperative effect · Triazine · Hydrogen bonds

## Introduction

The chemistry of non-covalent interactions, or supramolecular chemistry, is of enormous interest in material science research, in crystal engineering as well as in nanochemistry. It is accepted that this field constitutes a promising way to technological applications, covering areas of supramolecular polymers, smart materials, and molecular devices [1]. Much of the exploration in this field involves the use of 1,3,5-triazinane-2,4,6-trione or cyanuric acid (CA). This triazine-derivative has been most commonly known for their uses in swimming pools as a stabilizer [2, 3], since it combines with the free available chlorine to form trichloroisocyanuric acid, which acts as a sanitizer and is more stable against UV rays than free chlorine. Furthermore, due to its high structural similarity with RNA and DNA base pairs, such as uracil and thymine respectively, CA has also become an excellent candidate to be used in the research of supramolecular assemblies, with potential applications in the field of biology [4, 5] and materials science [6, 7].

It is known that CA can occur as two tautomer forms: the enol-like triazine-triol and the keto-like tautomer (See Fig. 1, **1** and **2**), which is more stable than the former [8–10]. Its singular features are due to their three hydrogen bond (H-bond) donor and three acceptor sites with the ability to form nine H-bonds at the same time, e.g., with Melamine (M) [11], and six H-bond with itself [12, 13]. In the field of crystalline materials and crystal engineering, there has been a marked research of

---

This paper belongs to Topical Collection QUITEL 2016

**Electronic supplementary material** The online version of this article (doi:10.1007/s00894-017-3428-3) contains supplementary material, which is available to authorized users.

✉ Nélica M. Peruchena  
arabeshai@fire.utn.edu.ar

✉ Gladis L. Sosa  
glrosa@fire.utn.edu.ar

<sup>1</sup> Grupo de Investigación en Química Teórica y Experimental (QuiTEx), Departamento de Ingeniería Química, Facultad Regional Resistencia, Universidad Tecnológica Nacional, French 414 (H3500CHJ), Resistencia, Chaco, Argentina

<sup>2</sup> Instituto de Química Básica y Aplicada del Nordeste Argentino (IQUIBA-NEA), UNNE-CONICET, Avenida Libertad 5460 (3400), Corrientes, Argentina

<sup>3</sup> Laboratorio de Estructura Molecular y Propiedades (LEMYP), Área de Química Física, Facultad de Ciencias Exactas y Naturales y Agrimensura, Universidad Nacional del Nordeste, Avenida Libertad 5460 (3400), Corrientes, Argentina

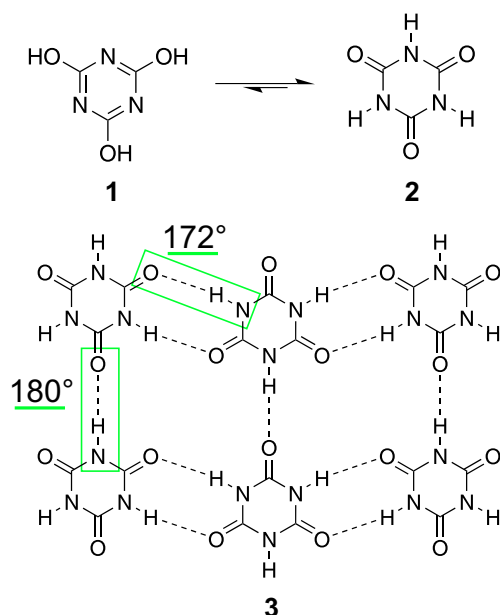


**Fig. 1** Structure of 1,3,5-triazine-2,4,6-triol **1**, structure of 1,3,5-triazinane-2,4,6-trione **2**, H-bond pattern of the CA crystal structure **3** [12]

CA co-crystals with a great variety of compounds like M [14, 15], 4,4'-bipyridyl [16], dimethylsulfoxide, dimethylamine, dimethylformamide [17], and some phenantrolines [18]. One of the co-founders of the bases of supramolecular chemistry and co-workers, Jean-Marie Lehn et al. [19], have synthesized a supramolecular helical structure based on a linear oligo-isophthalamide strand using CA as a template that directs the assembly process of the helix. Therefore, it is worthwhile to go on in this direction, since this topic still triggers a great scientific activity for the development of new materials.

The crystal structure of pure CA has been well studied since its resolution [12]. In the 3D structure the molecules are arranged by N–H···O H-bonds having two geometrical features, that is, N–H···O bond angles of 180° and 172.4° [12] (see Fig. 1, 3). Besides, if water is used as a crystallization solvent the CA hydrate is obtained [20], in which water molecules are placed coplanar with CA by interacting with three units via N–H···O (water as acceptor) and O–H···O (water as donor) H-bonds. The water molecules disrupt those N–H···O H-bonds of 172.4° between CA units, and just those ones of 180° remain. However, unlike the pure crystal, in the crystal hydrate the CA molecules are placed in the same position whereas in the dehydrated one, the molecules are inverted relative to one another (see Fig. 1, 3). Furthermore, Flynn et al. [13] have successfully obtained CA self-assembled monolayers on graphite. In this study, they have shown the coexistence of three new H-bond patterns beside the well-known arrangement of the 3D crystal structure. This behavior is partially explained by two energetic components: the electrostatic and the Lennard-Jones energy. They also suggest that the three domains are metastable configurations. However, the

nucleation process that originates these domains and their coexistence is not fully understood. Hence, knowing how to master the intermolecular forces involved in self-assembly strategies, requires further examination into the nature of the interactions between CA units. In addition, exploring the diversity of possible supramolecular arrangements is of great importance for structure prediction and design of new programmed structures.

In order to gain a deeper insight about how systems are reorganized by the possible combinations of H-bonds until they reach the most stable structures, we discuss different hydrogen bonding arrangements of CA supramolecules by analyzing complexes taken from literature and, as far as we know, molecular aggregates that have not been considered yet. In this work, we have performed a topological study via the quantum theory of atoms in molecules (QTAIM) and a natural bond orbital analysis (NBO) on several CA molecular assemblies.

## Computational methods

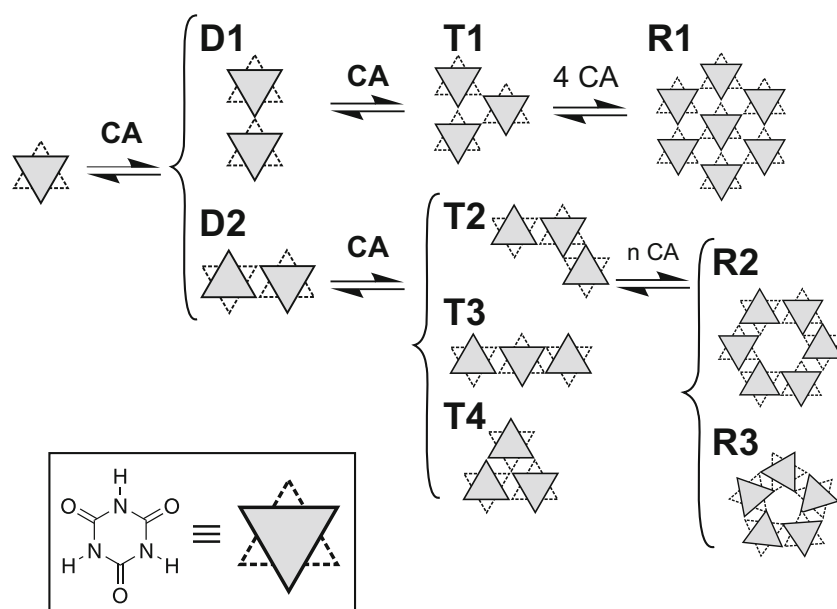
The set of complexes studied here were chosen as follows: three dimers (**D1**, **D2** and **D3**), four trimers (**T1**, **T2**, **T3**, and **T4**), two rosette type structures taken from Flynn's et al. work [13] (**R1** and **R2**) and a rosette type structure based on five CA units (**R3**). Finally, a molecular aggregate with the H-bond pattern of the pure crystal (Fig. 1, 3) was also studied. This last structure was taken from the crystallographic structure data obtained by Coppens and Vos [12]. According to the H-bond types, linear or double, the set of complexes can be arranged in an aggregation path which is shown in Fig. 2.

Geometries of CA<sub>n</sub> clusters (with  $n = 1, 2, 3, 5, 6, 7$ ) were manually assembled and fully optimized without any constraint using the GAMESS [21] quantum chemistry package. The optimizations were done using three levels of theory with the 6-311++G(d,p) basis set: the B3LYP hybrid functional [22, 23]; the B3LYP-D3 functional, which accounts for Grimme dispersion corrections [24]; and the  $\omega$ -B97XD hybrid functional from Head-Gordon et al. [25], which also includes empirical dispersion and correction designed for long-range interactions. The minimum energy nature of the optimized structures was verified using the vibrational frequency analysis. The binding energies  $\Delta E_{\text{bond}}$  (BE) were obtained at the same level of theory using the approach of Fonseca Guerra et al. [26–28], which is calculated as the sum between the interaction energy of the complex  $\Delta E_{\text{Int}}$  and the preparation energy  $\Delta E_{\text{Prep}}$  (Eq. 1).

$$\Delta E_{\text{bond}} = \Delta E_{\text{Int}} + \sum \Delta E_{\text{Prep}} \quad (1)$$

In this equation, the interaction energy  $\Delta E_{\text{Int}}$  is the difference between the energy of the complex and the sum of

**Fig. 2** Schematic representation of a hypothetical aggregation path



energies of the monomers within the structure of the complex. The preparation energy  $\Delta E_{\text{Prep}}$  is the difference between the energy of the monomer in the complex and the energy of its isolated structure, or in other words, is the deformation energy of each monomer upon complexation. The  $\Delta E_{\text{bond}}$  have also been corrected for the basis set superposition error (BSSE) within the approach of Boys and Bernardi [29].

The cooperativity ( $\Delta E_{\text{coop}}$ ) was calculated by Eq. 2 [30, 31].

$$\Delta E_{\text{coop}} = \Delta E_{\text{Int}}(CA_{n>2}) - \sum \Delta E_{\text{Int}}(CA_2) \quad (2)$$

where  $\Delta E_{\text{Int}}(CA_{n>2})$  is the total interaction energy of either trimers or rosettes and  $\sum \Delta E_{\text{Int}}(CA_2)$  is the sum of the interaction energies of the corresponding dimers (either **D1** or **D2**).

The synergy effect was also evaluated by Eq. 3 within the procedure of Fonseca Guerra et al. [27, 32].

$$\Delta E_{\text{Syn}} = \Delta E_{\text{Int}} - (\sum \Delta E_{\text{Pair}} + \sum \Delta E_{\text{Diag}}) \quad (3)$$

where  $\Delta E_{\text{Pair}}$  is the interaction between two molecules connected by H-bonds,  $\Delta E_{\text{Diag}}$  is the interaction between two non-H-bonded molecules in the complex, and  $\Delta E_{\text{Syn}}$  is the interaction synergy (cooperative effect) that takes place in the complex. Thus, if  $\Delta E_{\text{Syn}} < 0$ , a positive cooperative effect is present, whereas, if  $\Delta E_{\text{Syn}} > 0$ , the cooperativity is negative.

For the topological analysis, total electron densities were calculated at the B3LYP/6-311++G(d,p), level of theory. The local properties at bond critical points (BCP) were calculated using the AIMALL [33] program. The QTAIM of Bader [34] provides a rigorous definition of the chemical concepts of atom, bond, and structure. This theory has been used successfully for the characterization of H-bond interactions through a set of local topological properties calculated at BCP of

electron charge density. In this work, the electron charge density at the BCP,  $\rho_b$ , which measures the accumulation of charge between the bonded nuclei and reflects the bond strength; [35, 36] the Laplacian of the electron density  $\nabla^2 \rho_b$  that provides information about the local charge concentration ( $\nabla^2 \rho_b < 0$ ) or depletion ( $\nabla^2 \rho_b > 0$ ); the densities of kinetic energy  $G_b$ , the densities of potential energy  $V_b$ , and the total electronic energy density  $H_b = V_b + G_b$  were used to analyze the nature of the interactions that occur in the different complexes. Another parameter that describes a chemical bond is the delocalization index (DI(A,B)), which measures the average number of electrons delocalized between two atomic basins, A and B.

Finally, the optimized geometries computed at B3LYP/6-311++G(d,p) level of theory were used to perform a NBO analysis [37] from NBO 3.1 program [38] as implemented in Gaussian 03 [39]. This analysis was conducted to quantitatively evaluate the interactions of charge transfer (CT) involved in the formation of H-bonds and the cooperative effects.

## Results and discussion

### Geometric, energetic, and electron charge density analysis

Table S1 reports relevant optimized geometrical parameters of N–H $\cdots$ O interactions, such as H-bond lengths  $d_{\text{H}\cdots\text{O}}$ ,  $\theta_{\text{N-H}\cdots\text{O}}$  H-bonds angles, and the  $d_{\text{N-H}}$  proton-donor bond lengths. Due to the geometrical features of trimers and rosette complexes, the interactions are classified as *inner* and *outer*. Table 1 shows corrected BEs by BSSE obtained with the B3LYP, B3LYP-D3, and  $\omega$ -B97XD functionals.

**Table 1** Corrected binding energies  $\Delta E_{\text{bond}}$  by BSSE

Complexes	B3LYP	B3LYP-D3	$\omega$ -B97XD
<b>D1</b>	-5.67	-7.00 <sup>a</sup>	-6.75 <sup>b</sup>
<b>D2</b>	-11.37	-14.29	-13.73
<b>D3</b>	-6.12	-9.68	-9.32
<b>T1</b>	-18.40	-22.63 <sup>a</sup>	-21.88 <sup>b</sup>
<b>T2</b>	-22.87	-28.77	-27.66
<b>T3</b>	-22.63	-28.47	-27.30
<b>T4</b>	-21.61	-28.46	-27.34
<b>R1</b>	-71.87	-88.90 <sup>a</sup>	-85.81 <sup>b</sup>
<b>R2</b>	-69.12	-86.98	-83.56
<b>R3</b>	-53.52	-68.65	-66.05

All values in kcal mol<sup>-1</sup>. <sup>a</sup> B3LYP-D3/6-311++G\*\*//B3LYP/6-311++G\*\* single point results for comparison. <sup>b</sup>  $\omega$ -B97XD/6-311++G\*\*//B3LYP/6-311++G\*\* single point results for comparison

Optimization results slightly diverge for the three theoretical methods evaluated. In general, it is identified that the B3LYP-D3 and the  $\omega$ -B97XD functionals show longer  $d_{\text{N-H}}$  and shorter  $d_{\text{H-O}}$  distances compared with B3LYP calculations. It is also verified in all complexes that N-H distances are elongated as a consequence of complex formation, which is consistent with the formation of a conventional H-bond. In addition, as expected, BEs with dispersion correction are more negative than B3LYP calculations.

The following discussion is organized as follows: *dimers*, *trimers*, and *rosette*-like structures are discussed separately. Finally, *cooperative effects* are examined among all set of complexes.

### Dimers

Figure 3 shows the molecular graphs of the dimers obtained. The values of charge density at the H-bond BCPs,  $\rho_b$ , are also included. Three different configurations of H-bonded complexes can be seen in this figure. In **D1**, the N-H...O H-bond with an angle of 180° is verified; in **D2**, both CA units play a dual role as a proton acceptor and as a proton donor, with  $\theta_{\text{N-H...O}}$  values of 167.2° (close to the experimental value:  $\theta = 172.4^\circ$  [12]). Finally, in **D3**, the N-H...O H-bond shows an angle of 156.6°, which is less collinear than the previous ones. When considering optimizations, in the case of the functionals with dispersion correction, they do not predict a structure of **D1** complex, but it tends to adopt the conformation of **D2** complex. Moreover, the proposed T-shaped and parallel stacked arrangements have not been observed. Instead, the optimization of both structures unambiguously gives the **D3** structure, with either of the functionals. In this structure it can be seen that the carbonylic oxygen interacts with the positive region of the ring, as expected, which is confirmed by the presence of a C...O BCP.

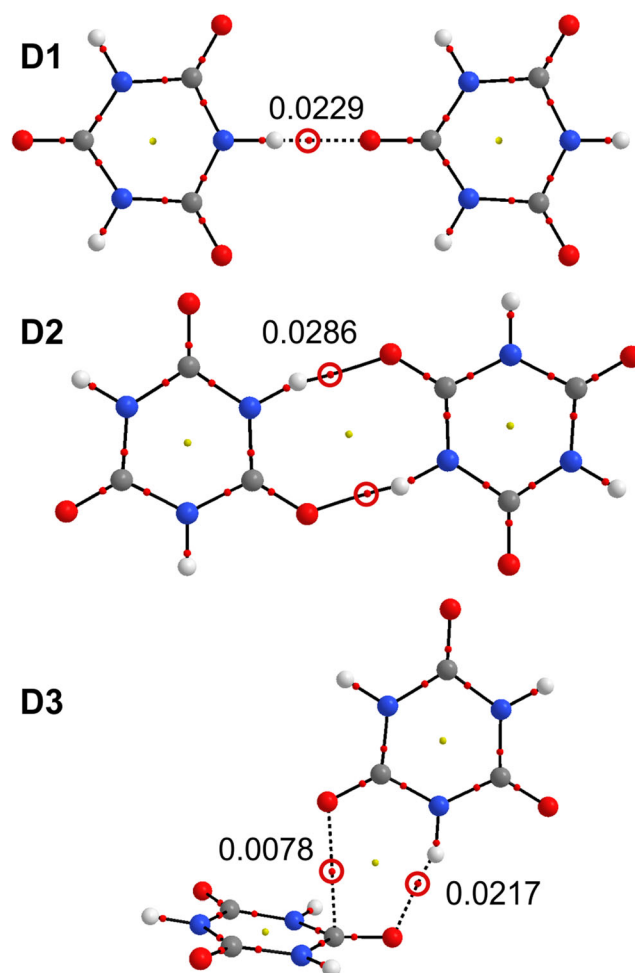


**Fig. 3** Molecular graphs of optimized dimers. The lines connecting the nuclei are the bond paths. Red circles are the BCPs or (3, -1) critical points, and yellow circles represent ring critical points or (3, +1) critical points. Values of  $\rho_b$  at BCPs, which were obtained at B3LYP level, are given in atomic units

Observation of the energetic analysis reported in Table 1 shows that BEs decrease in the following order: **D2** > **D3** > **D1**. It is important to note that  $\Delta E_{\text{bond}}$  (B3LYP) of complex **D2** is almost twice the  $\Delta E_{\text{bond}}$  (B3LYP) of complex **D1**; thus, it is difficult to establish what the primitive structure of **R1** is, and also to explain the energetic stabilities of **R1** and **R2** structures, since both arrangements were found to coexist [13]. Then, an interesting question arises: what is the mechanism by which H-bond arrangement of 180° is formed? The following sections intend to answer this question.

Detailed information of H-bonds, as well as other interactions, is obtained by the QTAIM analysis reported in Table 2. In all the complexes studied, values of  $\rho_b$  and  $\nabla^2\rho_b$  at the H-bond BCPs fall within the proposed range for closed shell interactions [40]. In addition,  $V_b$  and  $G_b$  are of the same order of magnitude, and  $H_b$  is positive and close to zero. On the basis of the local energy density parameters derived from the

**Table 2** Local topological properties at N–H···O BCPs

Complex	Interaction	$\rho_b$	$\nabla^2\rho_b$	$V_b$	$G_b$	$H_b$	DI(H,O)
<b>D1</b>	N–H···O	0.0229	0.1017	−0.0179	0.0217	0.0037	0.0678
<b>D2</b>	N–H···O	0.0286	0.1047	−0.0225	0.0243	0.0019	0.0849
	N–H···O	0.0287	0.1048	−0.0225	0.0244	0.0018	0.0850
<b>D3</b>	N–H···O	0.0217	0.0854	−0.0156	0.0185	0.0029	0.0656
	O···C	0.0078	0.0299	−0.0052	0.0063	0.0011	0.0187
<b>T1</b>	N–H···O	0.0266	0.1141	−0.0220	0.0253	0.0032	0.0765
<b>T2</b>	N–H···O <sub>outer</sub>	0.0285	0.1043	−0.0223	0.0242	0.0019	0.0847
	N–H···O <sub>inner</sub>	0.0291	0.1062	−0.0230	0.0248	0.0018	0.0859
<b>T3</b>	N–H···O	0.0283	0.1038	−0.0221	0.0240	0.0019	0.0841
<b>T4</b>	N–H···O <sub>outer</sub>	0.0282	0.1014	−0.0217	0.0235	0.0018	0.0848
	N–H···O <sub>inner</sub>	0.0283	0.1029	−0.0222	0.0239	0.0018	0.0841
	O···O	0.0010	0.0046	−0.0004	0.0008	0.0004	0.0076
<b>R1</b>	N–H···O <sub>outer</sub>	0.0247	0.1061	−0.0197	0.0231	0.0034	0.0721
	N–H···O <sub>inner</sub>	0.0283	0.1183	−0.0239	0.0268	0.0028	0.0805
<b>R2</b>	N–H···O <sub>outer</sub>	0.0287	0.1051	−0.0226	0.0244	0.0018	0.0849
	N–H···O <sub>inner</sub>	0.0286	0.1044	−0.0224	0.0243	0.0018	0.0849
<b>R3</b>	N–H···O <sub>outer</sub>	0.0218	0.0811	−0.0153	0.0178	0.0025	0.0685
	N–H···O <sub>inner</sub>	0.0334	0.1195	−0.0281	0.0290	0.0009	0.0940
<b>R4</b>	N–H···O <sub>outer</sub>	0.0247	0.1061	−0.0197	0.0231	0.0034	0.0721
	N–H···O <sub>inner</sub>	0.0283	0.1183	−0.0239	0.0268	0.0028	0.0805

All values in atomic units

QTAIM scheme,  $H_b$  has been used as a descriptor of covalent character when this property is negative [41, 42].

Furthermore, taking into account the values of  $\rho_b$  and DI(H,O), which are good indicators of the bond strength and bond order respectively; and because they are also strongly correlated [41, 42], the strongest interactions observed are those in the **D2** dimer, in line with the shortest  $d_{\text{H}\cdots\text{O}}$  distance and a highest binding energy. When topological parameters of **D1** and **D3** complexes are compared, the N–H···O H-bond of the **D1** complex is stronger than in the **D3** complex. However the later shows a second interaction between the carbonylic oxygen and the endocyclic carbon. This additional C···O interaction may favor the complex **D3** over **D1**.

### Trimers

As seen in dimers, the optimized structure of **T1** trimer obtained at B3LYP level is notably different from those obtained at B3LYP-D3 and  $\omega$ -B97XD levels. This is a consequence of dispersion corrections terms. The optimization with B3LYP-D3 and  $\omega$ -B97XD functionals tends to impose conformations that increase the number of intermolecular interactions. Figure 4a shows the molecular graph of the optimized **T1** complex using the B3LYP/6–311++G(d,p) level of theory. From this figure, one can infer that the complex keeps the  $\theta_{\text{N–H}\cdots\text{O}}$  angle close to 180° (see Table S1). In addition, when going from **D1** to **T1** geometry  $d_{\text{H}\cdots\text{O}}$  distances are shortened,

and the charge density at the BCPs,  $\rho_b$ , and DI(H,O) also increase (see Tables S1 and 2). Since the increase or decrease of  $\rho_b$  can be related to the cooperativity or negative cooperativity of H-bonds [31, 43], respectively, the observed changes indicate an enhancement of the H-bonds strength, and consequently a positive cooperativity. Figure 4b–c show the molecular graphs of the optimized **T1** complex using the B3LYP-D3/6–311++G(d,p) and the  $\omega$ -B97XD/6–311++G(d,p) levels of theory. Again, by comparison of these figures, they do not predict the expected arrangement. It can be seen that both functionals predict almost the same complexes and they just differ by the presence of an interaction of the type O···O (Fig. 4c).

What is more, both B3LYP-D3 and  $\omega$ -B97XD functionals predict an H-bond pattern with the same arrangement of the **D3** complex. At this point, it is important to highlight that although B3LYP is characterized by a lacking of London dispersion energy, it has shown an excellent performance in the calculation of geometries [44, 45], even with weak interactions like C–H···O HBs [46]. On the contrary, with regard to energy and thermochemistry calculations, it is widely known that dispersion corrected functionals give better results than non-corrected ones [44, 47]. In addition, it is known that corrected functionals tend to overestimate the binding [48]. For instance, in a study of the dimethylamine–trimethylphosphine complex, Kjaergaard et al. [49] have found that the B3LYP functional favors a structure with an

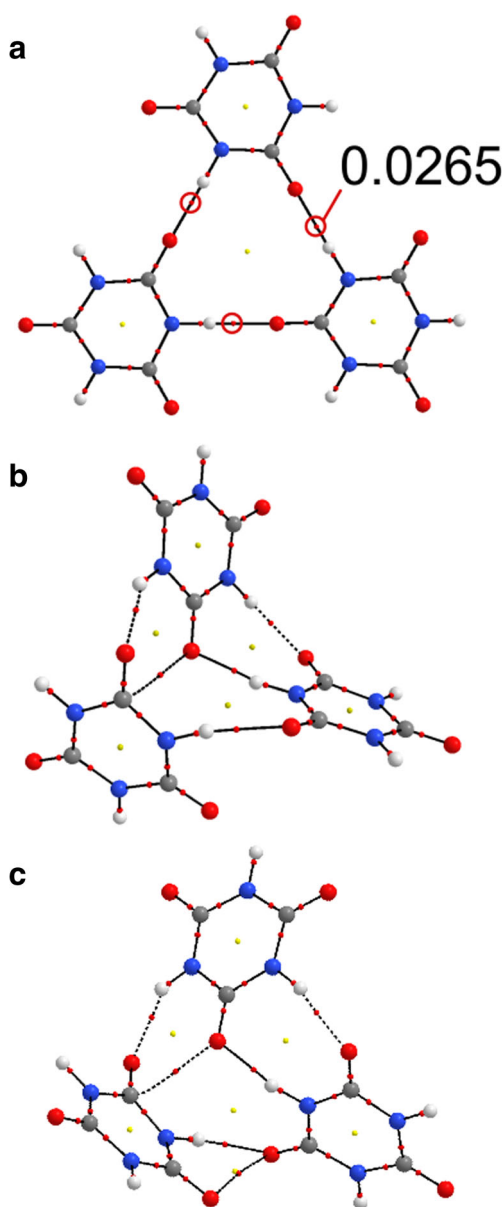


**Fig. 4** Molecular graphs of **T1** complexes **(a)** Structure optimized at B3LYP/6-311++G(d,p) level. The electron density at bond critical points is given in atomic units, all interactions are equivalent. **(b)** B3LYP-D3/6-311++G(d,p) geometry, **(c)**  $\omega$ -B97XD/6-311++G(d,p) geometry

N–H...P HB, while both B3LYP-D3 and  $\omega$ -B97XD functionals favor almost the same structure with both an N–H...P HB and C–H...N secondary interactions. In this work, the B3LYP functional is the best choice since it gives a reasonable reproduction of the experimental structure; and it is evident that the dispersion correction does not imply a better description of the systems because the long-range interactions seem to be less important. Finally, it is worth stressing that the **R1** rosette motif was obtained as a monolayer on both graphite [13] and Au(111) [50] surfaces, which also may affect the formation of the rosette.

Figure 5 shows the molecular graph of the optimized **T2** and **T3** complexes using the B3LYP/6-311++G(d,p) level of theory. By following the scheme of aggregation of Fig. 2, if more CA units are added to **T2** complex, a rosette-like structure (either **R2** or **R3**) is obtained. Besides, if more CA units are added to **T3** complex it will give an infinite linear arrangement. When going from **D2** to **T2** complex,  $d_{\text{H}\cdots\text{O}}$  distances of inner interactions are shortened, and likewise  $\rho_b$  and DI(H,O) increase (see Tables S1 and 2), which indicates a strengthening of these interactions. On the contrary, in the transition **D2**→**T3** all the interactions are weakened.

Finally, Fig. 6 shows the molecular graph of the optimized **T4** complex using the B3LYP/6-311++G(d,p) level of theory. In this case, either of the functionals employed predict the same geometry, with slight differences. This structure was not previously reported, and we consider that it constitutes an important part of the combinatorial library of CA complexes. In Fig. 6 the presence of a bifurcated H-bond can also be verified, in which an oxygen atom acts as a double proton acceptor. Topological values of these H-bonds do fall within the proposed range of Popelier [51]. In this arrangement, an interaction of the type O...O can also be seen, which can be classified as a van der Waals interaction [41].

Trends in BEs slightly differ between the functionals. For B3LYP and B3LYP-D3, BEs decrease in the following order: **T2** > **T3** > **T4** > **T1**, while for  $\omega$ -B97XD the trend is: **T2** > **T4** > **T3** > **T1**. The most stable structure is **T2**, however, the energy differences separating the group of complexes range from  $-0.2 \text{ kcal mol}^{-1}$  to  $-4.5 \text{ kcal mol}^{-1}$ . The largest difference is of  $\sim -4.5 \text{ kcal mol}^{-1}$  between **T1** and **T2**.

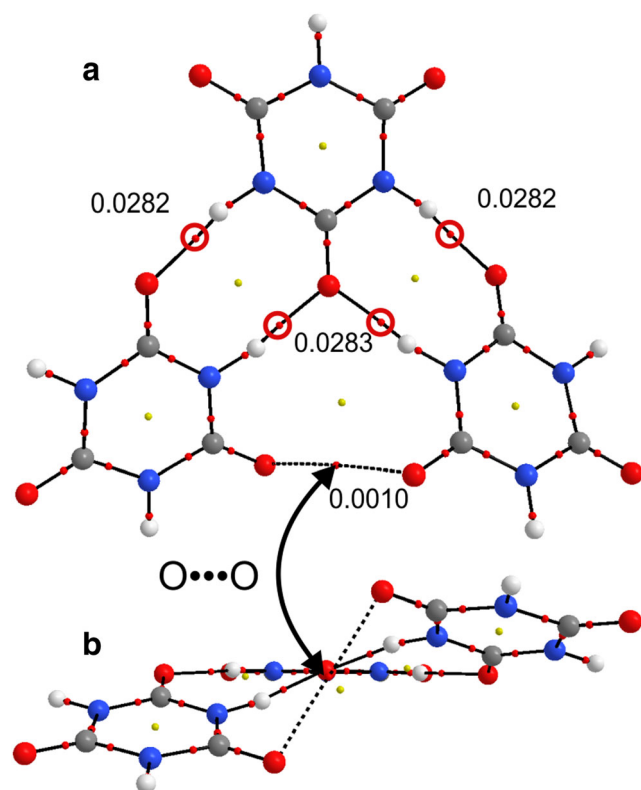
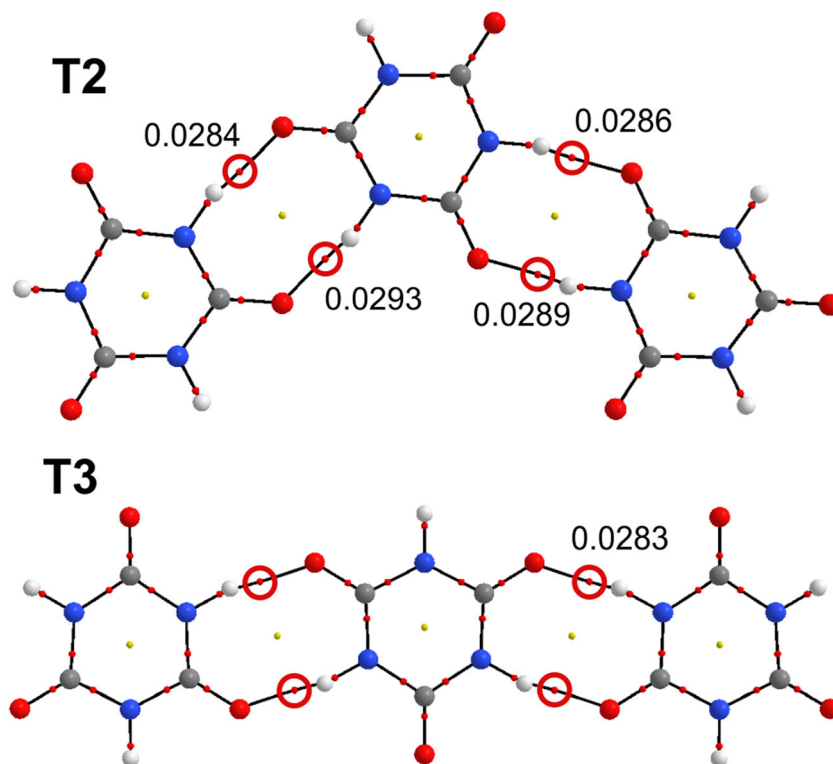
#### Rosettes

Figure 7 shows the molecular graph of the optimized **R1**, **R2**, and **R3** rosettes. Observation of these geometries shows that the most coplanar structure is **R2**, while **R1** complex shows some coplanarity but it seems to be unstable. Regarding **R3** complex, it shows a bowl-like structure alike the pentamer of metabolic acid [52]. Since **R2** and **R3** rosettes exhibit holes in their center with different sizes (4.3 Å and 3 Å respectively, for an isosurface density of  $\rho(r) = 0.001 \text{ au}$ ), they are good candidates to host ions with different sizes, just like quintets of uracil and thymine found by Qiu et al. [53].

When considering the **D1**→**T1**→**R1** evolution, the primitive N–H...O H-bond is enhanced in every step. That is, when going from **D1** to **R1**,  $d_{\text{H}\cdots\text{O}}$  distances are shortened and  $\rho_b$  and DI(H,O) values increase in magnitude. In addition, the inner interactions are more strengthened than the outer ones.

On the contrary, when considering the **D2**→**T2**→**R2** evolution, in general the inner N–H...O H-bonds are enhanced and the outer ones are weakened. For example, when going from **D2** to **T2**, the inner interactions are enhanced (from  $\rho_{\text{D2}} = 0.0286$  to  $\rho_{\text{T2}} = 0.0289 \sim 0.0293$ ). However, when

**Fig. 5** Molecular graphs of complexes **T2** and **T3**. Values of  $\rho_b$  at BCPs, which were obtained at B3LYP level, are given in atomic units



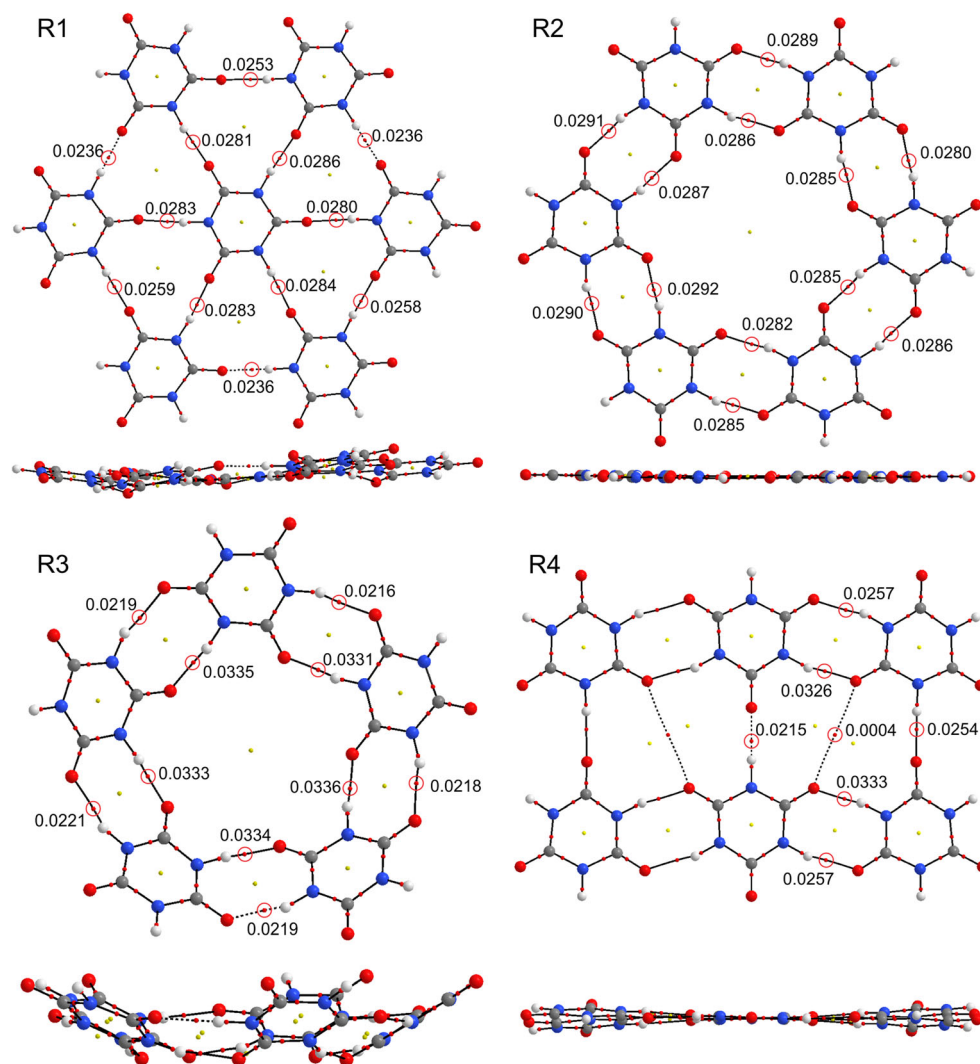
**Fig. 6** Molecular graph of the **T4** complex. (a) Top view. (b) Side view. Values of  $\rho_b$  at BCPs, which were obtained at the B3LYP level, are given in atomic units

going from **T2** to **R2**, this trend is not so clear in terms of the charge density analysis. When looking at the **T2**→**R3** transition, there is a clear enhancement of the inner interactions and the outer ones are weakened.

Despite that **R1** and **R2** complexes are geometrically different, they share the same number of interactions, which is 12 H-bonds. By comparing **R1** with **R2** complexes of Fig. 7, the H-bonds of **R2** complex are far stronger than interactions of **R1** complex (according  $\rho_b$  values). The sum of densities at H-bond BCPs is: 0.3175 au for **R1** complex and 0.3438 au for **R2** complex. This trend is in line with the interaction energies  $\Delta E_{\text{int}}$ . However, when looking at  $\Delta E_{\text{bond}}$  values, **R1** is almost 2.75 kcal mol<sup>-1</sup> stronger than **R2** (for B3LYP, and ~2 kcal mol<sup>-1</sup> for B3LYP-D3 and  $\omega$ -B97XD). Consequently, the positive cooperativity gains an enormous importance in these systems.

It is also interesting to examine the H-bond arrangement of the CA crystal structure (Fig. 7, **R4**). This H-bond pattern shows components of both rosettes **R1** and **R2**. That is, the H-bond pattern shows the presence of H-bonds with  $\theta_{\text{N-H}\cdots\text{O}}$  close to 180° and 172°. It is interesting to note that neither of the functionals predict the coplanar structure of the crystal, not even the B3LYP functional which is widely known to predict good geometries [43]. With regard to intermolecular interactions within the crystal, a BCP is evidenced between O atoms, as well as in previous complexes (**T1**/ $\omega$ -B97XD and **T4**). However, topological values ( $\rho_b$ ,  $\nabla^2\rho_b$ ,  $H_b$ ) indicate that this interaction is a van der Waals bonding. It should also be noted,

**Fig. 7** Top and side view of molecular graphs of **R1**, **R2**, **R3**, and **R4** complexes. Values of  $\rho_b$  at BCPs, which were at the B3LYP level, are given in atomic units



that the closed-shell  $O\cdots O$  interaction has been observed in several environments, going from ligand-receptor systems [54], silicates [55], the  $Mn_2(CO)_{10}$  complex [56], and in several derivatives of *cis*- $\beta$ -diketone [57]. Therefore, within the QTAIM methodology, this interaction is receiving increasing attention either in biological systems or in materials chemistry.

#### Cooperative effects

In order to evaluate the cooperativity from an energetic point of view, we compared the H-bond interactions in the trimers and rosettes with their similar counterparts in dimer complexes. Table 3 shows the energetic contribution due to cooperativity  $\Delta E_{coop}$ , as well as the synergy effect  $\Delta E_{Syn}$ .

The greatest gain of energy is observed in the series **D1**  $\rightarrow$  **T1** and **T1**  $\rightarrow$  **R1**. It is worth stressing that the three functionals predict almost the same trends of  $\Delta E_{coop}$  and  $\Delta E_{Syn}$ . On the contrary, the series of complexes **D2**  $\rightarrow$  **T2** and **T2**  $\rightarrow$  **R2** exhibit a lesser cooperative effect, which can be neglected. By

comparing **T1** and **T2** structures, **T1** has three  $N-H\cdots O$  H-bonds while **T2** has four. Also, **T2** is 4 kcal mol<sup>-1</sup> greater than **T1**, but the later shows a greater cooperative effect. Therefore, these structures can compete with each other during the self-assembly process.

Finally, the cooperative effect of **R3** rosette is fundamentally zero, which may explain the fact that it was not observed as a self-assembled monolayer. However, this structure could exist as a stable aggregate in solution since similar quintets have been observed between uracil molecules [53].

#### Critical points of $-\nabla^2\rho(r)$

The Laplacian of the electron density distribution,  $\nabla^2\rho(r)$ , is a powerful tool in the interpretation of molecular interactions. The topology of  $\nabla^2\rho(r)$ , in a molecular graph can also show the localization of basic and acidic regions [34, 58]. According to the  $L(r) = -1/4\nabla^2\rho(r)$  function, a (3, -3) critical point (CP) corresponds to a local maximum, and indicates a



**Table 3** Energetic contributions due to the cooperativity

Complexes	$\Delta E_{Coop}$			$\Delta E_{Syn}$		
	B3LYP	B3LYP-D3	$\omega$ -B97XD	B3LYP	B3LYP-D3	$\omega$ -B97XD
<b>T1</b>	-1.88	-2.09	-2.02	-1.52	-1.52	-1.43
<b>T2</b>	-0.09	-0.17	-0.11	0.02	0.01	0.03
<b>T3</b>	0.12	0.08	0.11	0.13	0.15	0.14
<b>T4</b>	0.97	-0.18	-0.06	-0.32	-0.30	-0.29
<b>R1</b>	-4.59	-5.76	-5.45	-4.73	-4.73	-4.43
<b>R2</b>	-0.38	-0.92	-0.75	0.20	0.15	0.19
<b>R3</b>	3.65	3.09	3.27	-0.08	-0.06	0.00

All values in kcal mol<sup>-1</sup>

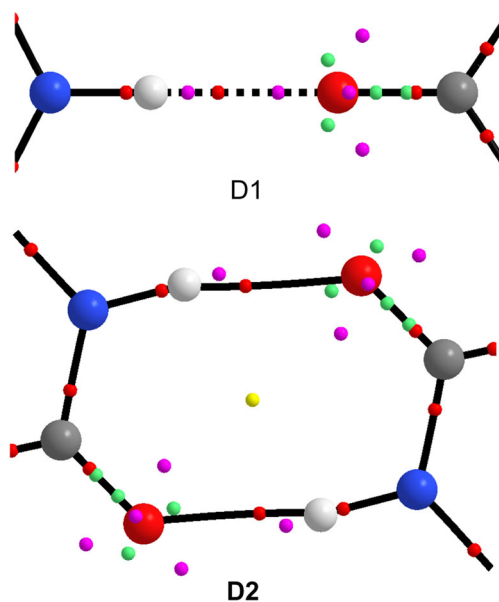
local electronic charge concentration. It has been shown that the maxima in  $L(r)$  are associated to electron pair domains of Lewis model [58]. Besides, a (3, +3) CP corresponds to a local minimum and indicates a local depletion of the electronic charge.

Figure 8 displays the (3, -3) and (3, +3) CPs in  $L(r)$ , superimposed on the molecular graph of **D1** and **D2** complexes. It can be immediately seen that in **D1** complex the molecules are oriented so that the minima in  $L(r)$  (pink circles), that corresponds to regions of charge depletion, are aligned, which explains why this arrangement is unstable. With regard to **D2** complex, Fig. 8 shows that this arrangement is stabilized by the well-known hole-lump interaction: a maxima of charge concentration is aligned with a minima of

charge depletion. The latter case is the most energetically favored.

### Natural bond orbital analysis

The cooperativity of H-bonds can also be analyzed from the viewpoint of hyperconjugative energies of charge transfer (CT) between NBOs. The results of NBO analysis conducted on CA complexes are given in Table 4. The values reported in this table are the second-order perturbation energies ( $E^{(2)}$ ) (donor→acceptor) that involve the oxygen lone pairs (LP) 1 and 2 and the N-H  $\sigma^*$  antibonds ( $n_{O} \rightarrow \sigma^*_{N-H}$ ). By analyzing these results the cooperativity can be clearly seen. In the **D1**→**T1**→**R1** transition, an augmentation of  $E^{(2)}$  values is evidenced. The inner interactions undergo a strong enhancement.



**Fig. 8** Critical points of the  $L(r)$  function superimposed on molecular graph of **D1** and **D2** complexes. Lines connecting the nuclei are the bond paths. Red circles are BCPs or (3, -1) critical points in  $\rho(\mathbf{r})$  function, yellow circles are ring critical points or (3, +1) critical points in  $\rho(\mathbf{r})$  function, green circles are (3, -3) critical points in  $L(r)$  function, and pink circles are (3, +3) critical points in  $L(r)$  function

**Table 4** Average second-order perturbation energies  $E^{(2)}$  (donor→acceptor) involving contributions of lone pairs (LP) 1 and 2 to  $\sigma^*$  antibonds:  $LP1_{O} \rightarrow \sigma^*_{(N-H)}$  and  $LP2_{O} \rightarrow \sigma^*_{(N-H)}$  interactions

Complex	Interaction	$E^{(2)}$	
		LP1	LP2
<b>D1</b>	N-H...O	9.13	0.00
<b>T1</b>	N-H...O	11.78	0.00
<b>R1</b>	N-H...O <sub>inner</sub>	12.90	< 0.1
	N-H...O <sub>outer</sub>	9.87	< 0.1
<b>D2</b>	N-H...O	6.93	7.52
	N-H...O	6.91	7.50
<b>T2</b>	N-H...O <sub>inner</sub>	6.79	5.31
	N-H...O <sub>outer</sub>	6.27	7.76
<b>T3</b>	N-H...O <sub>inner</sub>	7.21	7.68
	N-H...O <sub>outer</sub>	6.87	7.46
<b>T4</b>	N-H...O	6.81	7.33
	N-H...O	6.81	7.33
<b>R2</b>	N-H...O <sub>inner</sub>	7.17	7.44
	N-H...O <sub>outer</sub>	6.97	7.45
<b>R3</b>	N-H...O <sub>inner</sub>	8.97	8.32
	N-H...O <sub>outer</sub>	4.33	4.59

All values in kcal mol<sup>-1</sup>

Since the  $N-H\cdots O$  is strongly directional, it is observed that the LP2 does not participate in the CT interaction.

On the other hand, when looking at both **D2**→**T3** and **D2**→**T4** transitions, no increase is observed in  $E^{(2)}$  energies, but, **T2** structure exhibits an enhancement of inner interactions, as well as the **R2** rosette. Finally, when looking at the **D2**→**T2**→**R3** transition, the **R3** rosette displays a strong increment of  $E^{(2)}$  energies on inner interactions, while the outer ones display the opposite effect. Thus, these cooperative and anti-cooperative effects compensate each other and the total binding energy results being less than the sum of the parts, that is, a negative cooperativity.

### The origin of the cooperativity

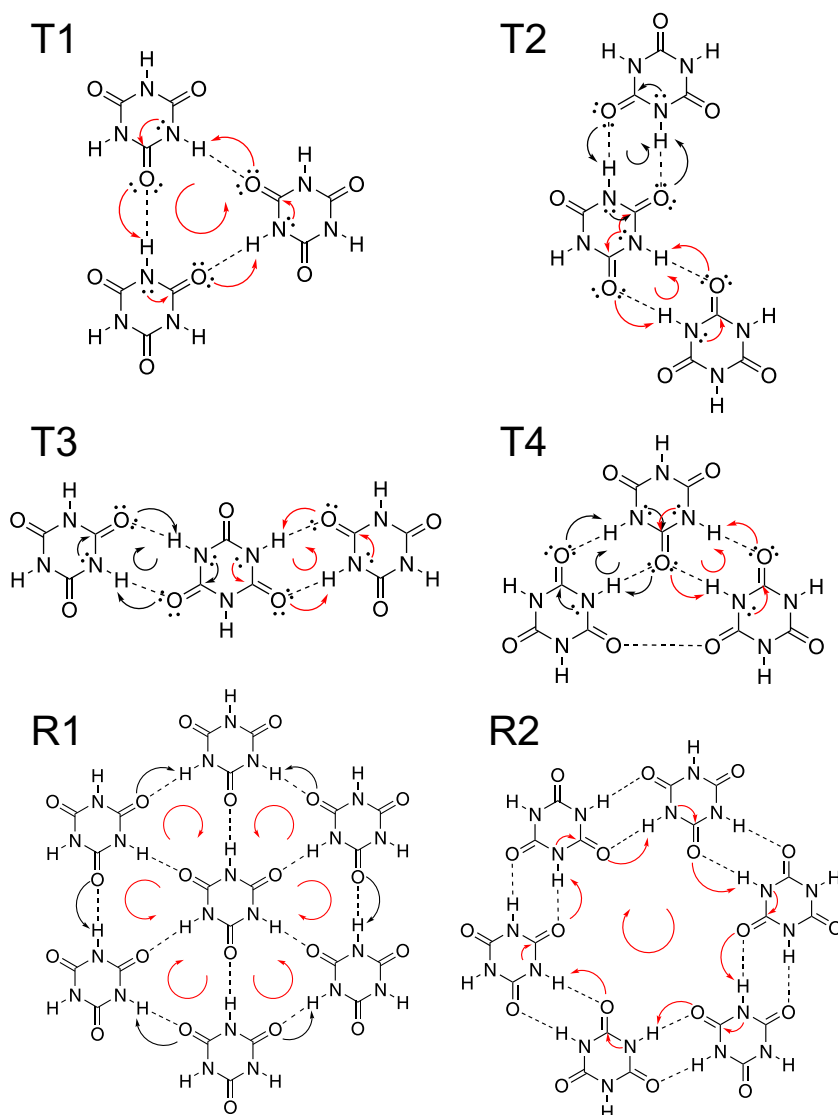
In our previous study on *M/CA* complexes [59], we showed that the  $n_N \rightarrow \sigma^*_{(C=O)}$  intramolecular CTs experience an increase of  $E^{(2)}$  energies upon complex formation. The charge

flows through both inter and intramolecular interactions like in a “circuit”. This effect is also present in *CA* supramolecules, as visualized in Fig. 9. This figure outlines the intra and intermolecular CTs between NBOs:  $n_N \rightarrow \sigma^*_{(C=O)}$  and  $n_O \rightarrow \sigma^*_{(N-H)}$ . It can be seen that in **T1** complex, the H-bonds point in one direction and there is a direct path that connects the three molecules involving  $n_N \rightarrow \sigma^*_{(C=O)}$  and  $n_O \rightarrow \sigma^*_{(N-H)}$  CTs. Contrarily, when looking at **T2**, **T3**, and **T4** complexes there is no such direct path that connects the molecular units. Besides, the H-bonds point in opposite directions.

When going from **T1** to **R1**, the inner interactions are reinforced because each  $C=O$  bond from the central unit receives charge from two nitrogen LPs. Moreover, the interactions of the outer periphery are weaker than the inner ones because there is not a direct path that connects them, in fact the H-bonds are in opposite directions.

With regard to the **T2** → **R2** transition, a direct path that connects  $n_N \rightarrow \sigma^*_{(C=O)}$  and  $n_O \rightarrow \sigma^*_{(N-H)}$  CTs is manifested

**Fig. 9** Schematic representation of  $n \rightarrow \sigma^*$  inter ( $n_O \rightarrow \sigma^*_{(N-H)}$ ) and intramolecular ( $n_N \rightarrow \sigma^*_{(C=O)}$ ) charge transfers involving interactions in *CA* trimers and rosettes. Circular arrows indicate the net charge flow as a consequence of  $n_O \rightarrow \sigma^*_{(N-H)}$  and  $n_N \rightarrow \sigma^*_{(C=O)}$  charge transfers



with the completion of the rosette, which explains why the inner interactions are stronger than the outer ones (either in **R2** or **R3** complexes).

These results are in good accordance with an earlier work of Fonseca Guerra et al. [27], in which they showed that supramolecules of guanine display a cooperativity effect that is absent in xanthine ones. This effect originates in the  $\sigma$ -electron system. The charge goes from one unit to the other in one direction. They have also argued that their model is expected to apply to other hydrogen-bonded supramolecules.

## Conclusions

In this work, a structural and an electronic analyses at B3LYP, B3LYP-D3, and  $\omega$ -B97XD/6-311++G(d,p) levels of theory were carried out on a series of supramolecular complexes formed by hydrogen bonds. A variety of possibilities have been shown in which CA can be arranged through H-bonds, that is, a combinatorial library of complexes. It is evident, that the formation of complex structures of CA involves an intricate path of supramolecular arrangements from the beginning of the self-assembly process. The B3LYP functional has shown the best performance to describe the interactions.

CA is a very versatile building block because it can form at least four rosette-like structures with different degrees of cooperativity. Since different organizations of the same building block show special energetic and topological features, it is a fact that they would lead to different functionalities and thus different macroscopic properties. For instance, **R2** and **R3** supramolecules could hold different cations with different ionic radii.

The energetic, topological, and NBO results demonstrate that the structures with  $\theta_{\text{N-H}\cdots\text{O}} = 180^\circ$  (**T1** and **R1**) display the highest cooperative effect. However, some structures with double H-bonds show greater binding energies but very low or zero cooperative effects. Therefore, they may compete with each other during the self-assembly steps, which may explain why all of these structures coexist in the same monolayer. The next ultimate challenge will be to obtain pure arrangements as self-assembled monolayers. It is also interesting to highlight that a greater cooperative effect is not always associated with a greater binding energy. The intramolecular charge transfers play a key role in the cooperative effect.

Finally, it is suggested that the nucleation process of **R1** rosette motif (with all  $\theta_{\text{N-H}\cdots\text{O}}$  close to  $180^\circ$ ) cannot be originated from **D1** dimer ( $\theta_{\text{N-H}\cdots\text{O}} = 180^\circ$ ), since it is a very unstable structure and its cyclic analogue (**D2**), which has two H-bonds, is twice more stable. Therefore, the **T1** structure could be originated as a concerted assembly process, and the **R1** rosette originated from the **T1** structure.

**Acknowledgments** Grants from Secretaría de Ciencia y Tecnología, Universidad Tecnológica Nacional, Facultad Regional Resistencia supported this work. A.N.P. thanks National Scientific and Technical Research Council (CONICET), Argentina, for a doctoral fellowship. N.M.P. is a CONICET career researcher.

## References

1. Ariga K, Hill JP, Lee MV, Vinu A, Charvet R, Acharya S (2008) Challenges and breakthroughs in recent research on self-assembly. *Sci Technol Adv Mater* 9:14109. doi:10.1088/1468-6996/9/1/014109
2. Downes CJ, Mitchell JW, Viotto ES, Eggers NJ (1984) Determination of cyanuric acid levels in swimming pool waters by u.v. Absorbance, HPLC and melamine cyanurate precipitation. *Water Res* 18:277–280. doi:10.1016/0043-1354(84)90100-3
3. Cantú R, Evans O, Kawahara FK, Wymer LJ, Dufour AP (2001) HPLC determination of cyanuric acid in swimming pool waters using phenyl and confirmatory porous graphitic carbon columns. *Anal Chem* 73:3358–3364. doi:10.1021/ac001412t
4. Ma M, Gong Y, Bong D (2009) Lipid membrane adhesion and fusion driven by designed, minimally multivalent hydrogen-bonding lipids. *J Am Chem Soc* 131:16919–16926
5. Avakyan N, Greschner AA, Aldaye F, Serpell CJ, Toader V, Petitjean A, Sleiman HF (2016) Reprogramming the assembly of unmodified DNA with a small molecule. *Nat Chem* 1–9. doi:10.1038/nchem.2451
6. Yagai S, Nakajima T, Karatsu T, Saitow K, Kitamura A (2004) Phototriggered self-assembly of hydrogen-bonded rosette. *J Am Chem Soc* 126:11500–11508. doi:10.1021/ja047783z
7. Liu Y, Wang Q (2006) Melamine cyanurate-microencapsulated red phosphorus flame retardant unreinforced and glass fiber reinforced polyamide 66. *Polym Degrad Stab* 91:3103–3109. doi:10.1016/j.polymdegradstab.2006.07.026
8. Mukherjee S, Ren J (2010) Gas-phase acid-base properties of melamine and cyanuric acid. *J Am Soc Mass Spectrom* 21:1720–1729. doi:10.1016/j.jasms.2010.06.002
9. Pérez-Manríquez L, Cabrera A, Sansores LE, Salcedo R (2011) Aromaticity in cyanuric acid. *J Mol Model* 17:1311–1315. doi:10.1007/s00894-010-0825-2
10. Klotz IM, Askounis TJ (1947) Absorption spectra and Tautomerism of Cyanuric acid, melamine and some related compounds. *J Am Chem Soc* 69:801
11. Ranganathan A, Pedireddi VR, Rao CNR (1999) Hydrothermal synthesis of Organic Channel structures: 1:1 hydrogen-bonded adducts of melamine with cyanuric and trithiocyanuric acids. *J Am Chem Soc* 121:1752–1753
12. Coppens P, Vos A (1971) Electron density distribution in cyanuric acid. II. Neutron diffraction study at liquid nitrogen temperature and comparison of X-ray neutron diffraction results. *Acta Crystallogr B* 27:146–158. doi:10.1107/S0567740871001808
13. Kannappan K, Werblowsky TL, Rim KT, Berne BJ, Flynn GW (2007) An experimental and theoretical study of the formation of nanostructures of self-assembled Cyanuric acid through hydrogen bond networks on graphite. *J Phys Chem B* 111:6634–6642
14. Choi IS, Li X, Simanek EE, Akaba R, Whitesides GM (1999) Self-assembly of hydrogen-bonded polymeric rods based on the Cyanuric acid-melamine lattice. *Chem Mater* 11:684–690. doi:10.1021/cm980540j
15. Prior TJ, Armstrong JA, Benoit DM, Marshall KL (2013) The structure of the melamine–cyanuric acid co-crystal. *CrystEngComm* 15:5838. doi:10.1039/c3ce40709h

16. Ranganathan A, Pedireddi VR, Sanjayan G, Ganesh KN, Rao CNR (2000) Sensitive dependence of the hydrogen-bonded assemblies in cyanuric acid–4,4'-bipyridyl adducts on the solvent and the structure of the parent acid. *J Mol Struct* 522:87–94
17. Pedireddi VR, Belhekar D (2002) Investigation of some layered structures of cyanuric acid. *Tetrahedron* 58:2937–2941
18. Marivel S, Suresh E, Pedireddi VR (2008) Molecules to supermolecules and self assembly: a study of some cocrystals of cyanuric acid. *Tetrahedron Lett* 49:3666–3671. doi:10.1016/j.tetlet.2008.03.143
19. Berl VV, Krische MJ, Huc I, Lehn JM, Schmutz M (2000) Template-induced and molecular recognition directed hierarchical generation of supramolecular assemblies from molecular strands. *Chem Eur J* 6:1938–1946. doi:10.1002/1521-3765(20000602)6:11<1938::aid-chem1938>3.0.co;2-y
20. Lewis TC, Tocher DA, Price SL (2005) Investigating unused hydrogen bond acceptors using known and hypothetical crystal polymorphism. *Cryst Growth Des* 5:983–993
21. Schmidt MW, Baldrige KK, Boatz JA, Elbert ST, Gordon MS, Jensen JH, Koseki S, Matsunaga N, Nguyen KA, Su S, Windus TL, Dupuis M, Montgomery JA (1993) General atomic and molecular electronic structure system. *J Comput Chem* 14:1347–1363
22. Becke AD (1993) Density-functional thermochemistry. III. The role of exact exchange. *J Chem Phys* 98:5648–5652
23. Lee C, Yang W, Parr RG (1988) Development of the Colle-Salvetti correlation-energy formula into a functional of the electron density. *Phys Rev B* 37:785–789
24. Grimme S, Antony J, Ehrlich S, Krieg H (2010) A consistent and accurate ab initio parametrization of density functional dispersion correction (DFT-D) for the 94 elements H–Pu. *J Chem Phys* 132:154104. doi:10.1063/1.3382344
25. Chai J-D, Head-Gordon M (2008) Long-range corrected hybrid density functionals with damped atom-atom dispersion corrections. *Phys Chem Chem Phys* 10:6615–6620
26. Fonseca Guerra C, van der Wijst T, Bickelhaupt FM (2005) Substituent effects on hydrogen bonding in Watson–Crick Base pairs. A theoretical study. *Struct Chem* 16:211–221. doi:10.1007/s11224-005-4453-x
27. Fonseca Guerra C, Zijlstra H, Paragi G, Bickelhaupt FM (2011) Telomere structure and stability: Covalency in hydrogen bonds, not resonance assistance, causes cooperativity in guanine quartets. *Chem A Eur J* 17:12612–12622. doi:10.1002/chem.201102234
28. Paragi G, Kupihár Z, Guerra CF, Bickelhaupt FM, Kovács L (2012) Supramolecular ring structures of 7-methylguanine: a computational study of its self-assembly and anion binding. *Molecules* 18:225–235. doi:10.3390/molecules18010225
29. Boys SF, Bernardi F (1970) The calculation of small molecular interactions with the differences of separate total energies. Some procedures with reduced errors. *Mol Phys* 19:553–559
30. Dannenberg JJ (2006) Enthalpies of hydration of N-methylacetamide by one, two, and three waters and the effect upon the C=O stretching frequency. An Ab initio DFT study. *J Phys Chem A* 110:5798–5802. doi:10.1021/jp060452j
31. Angelina EL, Peruchena NM (2011) Strength and nature of hydrogen bonding interactions in mono- and di-hydrated formamide complexes. *J Phys Chem A* 115:4701–4710. doi:10.1021/jp1105168
32. Dominikowska J, Bickelhaupt FM, Palusiak M, Fonseca Guerra C (2016) Source of Cooperativity in halogen-bonded Haloamine tetramers. *ChemPhysChem* 17:474–480. doi:10.1002/cphc.201501130
33. AIMAll Version 12.06.03, Keith Todd A (2012) TK Gristmill Software, Overland Park KS, USA [aim.tkgristmill.com](http://aim.tkgristmill.com)
34. Bader RFW (1994) *Atoms in molecules: a quantum theory*. Clarendon Press, Oxford
35. Boyd RJ, Choi SC (1986) Hydrogen bonding between nitriles and hydrogen halides and the topological properties of molecular charge distributions. *Chem Phys Lett* 129:62–65. doi:10.1016/0009-2614(86)80169-5
36. Carroll MT, Bader RFW (1988) An analysis of the hydrogen bond in BASE-HF complexes using the theory of atoms in molecules. *Mol Phys* 65:695–722
37. Reed EA, Curtis AL, Weinhold F (1988) Intermolecular interactions from a natural bond orbital, donor-acceptor viewpoint *Chem Rev* 88:899–926
38. Glendening ED, Reed AE, Carpenter JE, Weinhold F (1998) NBO Version 3.1. TCI, University of Wisconsin, Madison
39. Frisch MJ, Trucks GW, Schlegel HB, Scuseria GE, Robb MA, Cheeseman JR, Montgomery Jr JA, Vreven T, Kudin KN, Burant JC, Millam JM, Iyengar SS, Tomasi J, Barone V, Mennucci B, Cossi M, Scalmani G, Rega N, Petersson GA, Nakatsuji H, Hada M, Ehara M, Toyota K, Fukuda R, Hasegawa J, Ishida M, Nakajima T, Honda Y, Kitao O, Nakai H, Klene M, Li X, Knox JE, Hratchian HP, Cross JB, Bakken V, Adamo C, Jaramillo J, Gomperts R, Stratmann RE, Yazyev O, Austin AJ, Cammi R, Pomelli C, Ochterski JW, Ayala PY, Morokuma K, Voth GA, Salvador P, Dannenberg JJ, Zakrzewski VG, Dapprich S, Daniels AD, Strain MC, Farkas O, Malick DK, Rabuck AD, Raghavachari K, Foresman JB, Ortiz JV, Cui Q, Baboul AG, Clifford S, Cioslowski J, Stefanov BB, Liu G, Liashenko A, Piskorz P, Komaromi I, Martin RL, Fox DJ, Keith T, Al-Laham MA, Peng CY, Nanayakkara A, Challacombe M, Gill PMW, Johnson B, Chen W, Wong MW, Gonzalez C, Pople JA (2004) Gaussian 03, revision D.01. Gaussian, Wallingford
40. Koch U, Popelier PLA (1995) Characterization of C–H–O hydrogen bonds on the basis of the charge density. *J Phys Chem* 99:9747–9754. doi:10.1021/j100024a016
41. Matta CF, Boyd RJ (2007) *The quantum theory of atoms in molecules: from solid state to DNA and drug design*. Wiley-VCH, Weinheim
42. Matta CF (2014) Modeling biophysical and biological properties from the characteristics of the molecular electron density, electron localization and delocalization matrices, and the electrostatic potential. *J Comput Chem* 35:1165–1198. doi:10.1002/jcc.23608
43. Petelski AN, Peruchena NM, Sosa GL (2016) Evolution of the hydrogen-bonding motif in the melamine–cyanuric acid co-crystal: a topological study. *J Mol Model* 22:202. doi:10.1007/s00894-016-3070-5
44. Filipe SS, Fernandes PA, Ramos MJ (2007) General performance of density functionals. *J Phys Chem A* 111:10439–10452
45. Tsepis AC (2014) DFT flavor of coordination chemistry. *Coord Chem Rev* 272:1–29. doi:10.1016/j.ccr.2014.02.023
46. Scheiner S (2015) Dissection of the factors affecting formation of a C–H···O H-bond. A case study. *Crystals* 5:327–345. doi:10.3390/cryst5030327
47. Fonseca Guerra C, van der Wijst T, Poater J, Swart M, Bickelhaupt FM (2010) Adenine versus guanine quartets in aqueous solution: dispersion-corrected DFT study on the differences in  $\pi$ -stacking and hydrogen-bonding behavior. *Theor Chem Accounts* 125:245–252. doi:10.1007/s00214-009-0634-9
48. Thanthiruwatte KS, Hohenstein EG, Burns LA, Sherrill CD (2011) Assessment of the performance of DFT and DFT-D methods for describing distance dependence of hydrogen-bonded interactions. *J Chem Theory Comput* 7:88–96
49. Möller KH, Hansen AS, Kjaergaard HG (2015, 119) Gas phase detection of the NH–P hydrogen bond and importance of secondary interactions. *J Phys Chem A*:10988–10998. doi:10.1021/acs.jpca.5b08358
50. Staniec PA, Perdigão LMA, Rogers BL, Champness NR, Beton PH (2007) Honeycomb networks and chiral superstructures formed by

- cyanuric acid and melamine on Au(111). *J Phys Chem C* 111:886–893. doi:10.1021/jp064964+
51. Popelier PLA (1998) Characterization of a Dihydrogen bond on the basis of the electron density. *J Phys Chem A* 102:1873–1878
52. Elango M, Subramanian V, Sathyamurthy N (2008) The self-assembly of metaboric acid molecules into bowls, balls and sheets. *J Phys Chem A* 112:8107–8115. doi:10.1021/jp8019254
53. Qiu B, Liu J, Qin Z, Wang G, Luo H (2009) Quintets of uracil and thymine: a novel structure of nucleobase self-assembly studied by electrospray ionization mass spectrometry. *Chem Commun* 2863–2865. doi:10.1039/b903857d
54. Andujar SA, Tosso RD, Suvire FD, Angelina E, Peruchena N, Cabedo N, Cortes D, Enriz RD (2012) Searching the “biologically relevant” conformation of dopamine: a computational approach. *J Chem Inf Model* 52:99–112. doi:10.1021/ci2004225
55. Gibbs GV, Downs RT, Cox DF, Ross NL, Boisen MB, Rosso KM (2008) Shared and closed-shell O–O interactions in silicates. *J Phys Chem A* 112:3693–3699. doi:10.1021/jp076396j
56. Bianchi R, Gervasio G, Marabello D (2000) Experimental electron density analysis of  $\text{Mn}_2(\text{CO})_{10}$ : metal–metal and metal–ligand bond characterization. *Inorg Chem* 39:2360–2366
57. Pakiari AH, Eskandari K (2007) Closed shell oxygen–oxygen bonding interaction based on electron density analysis. *J Mol Struct THEOCHEM* 806:1–7. doi:10.1016/j.theochem.2006.10.008
58. Bader RFW, Johnson S, Tang T-H (1996) The electron pair. *J Phys Chem* 100:15398–15415
59. Petelski AN, Duarte DJR, Pamies SC, Peruchena NM, Sosa GL (2016) Intermolecular perturbation in the self-assembly of melamine. *Theor Chem Accounts* 135:65. doi:10.1007/s00214-015-1795-3